

# Forming Simulation of Tailored Press Hardened Parts

Marcel Triebus<sup>1</sup>, Alexander Reitz<sup>2</sup>, Olexandr Grydin<sup>2</sup>, Julian Grenz<sup>3</sup>, Andreas Schneidt<sup>3</sup>, Rüdiger Erhardt<sup>3</sup>, Thomas Tröster<sup>1</sup>, Mirko Schaper<sup>2</sup>

<sup>1</sup> Paderborn University, Automotive Lightweight Design, Warburger Str. 100,  
33098 Paderborn, Germany

<sup>2</sup> Paderborn University, Material Science, Warburger Str. 100,  
33098 Paderborn, Germany

<sup>3</sup> BENTELER Automobiltechnik GmbH, An der Talle 27-31,  
33102 Paderborn, Germany

## Abstract

Hot forming of metal parts is characterized by forming over recrystallisation temperature [1]. For steel, press hardening is a popular production technology for creating hardened parts under hot forming conditions. In the conventional press hardening process, the blank is heated above austenitizing temperature and then transferred to the forming tool. The tools are water cooled and therefore ensure a martensitic transformation of the steel material. The most popular alloy is the boron steel 22MnB5, where a tensile strength of around 1500 MPa is reached through press hardening processes. The latest body-in-white concepts show a broad range of press hardened parts. The underlying forming methods are aiming to create purpose build components through variations of the press hardening process like tailored property processes, the use of tailor-welded or tailor-rolled blanks [2]. In the tailored property process, tailoring of the material properties is realized through the decrease of the cooling rate in a designated area of the part e.g., with a heated tool region. Due to the lower cooling rate, a softer and more ductile state is created in this area with microstructures of ferrite, pearlite and bainite. As a result, from the multiphase microstructure of tailored property parts, shape distortion is more pronounced than in conventional press hardening parts with a fully martensitic microstructure. Increased shape distortion can lead to additional rework cycles in the tool manufacturing.

This research proposes a method for simulation-based prediction of shape distortion to reduce rework. For the thermo-mechanical coupled simulation of the tailored-property process the phase transformations are considered with the material model **\*MAT\_248** [3]. The parameter identification for **\*MAT\_248** is done with dilatometer experiments and metallurgical evaluation of the resulting microstructure. The simulations show a good agreement with the experimental results for tailored property parts regarding the microstructure. Moreover, the predicted geometry of the parts after the forming process is validated with optical measurements.

## 1 Introduction

Press hardening is a popular hot forming production technology to create high-strength steel components for body-in-white structures. The most common alloy for press hardening is the boron steel 22MnB5, where a tensile strength of around 1500 MPa is reached through press hardening processes. Recent body-in-white concepts, like the Audi Q4 e-tron (2021), have an amount of 26 percent of hot formed steel components. A safety cell made of hot formed steel components ensures a high crash integrity for the passenger area during crash load cases [4]. In the conventional direct press hardening process, the blanks are heated above austenitization temperature and then transferred to a water-cooled tool. Due to the fast cooling-rate, the martensite transformation takes place during the forming and quenching step. While the conventional press hardening process is widely distributed nowadays, recent developments show variations of the press hardening process like the tailored property process. Tailored material properties can be established by different heating or cooling methods e.g., through partial austenitization or with heated tool regions. With slower cooling rates at designated areas of the steel component, the martensitic transformation is avoided and softer microstructures like ferrite, pearlite and bainite are evolving. These softer phases show an increased ductility. E.g., for an automotive b-pillar the ductile region is used at the bottom area to lead the maximum deformation in a side crash impact into the bottom structure and keep the passenger cell intact [5].

Another possibility for the variation of the press hardening process is the application of patched blanks. A patch is connected to the main pillar blank before the forming process via spotwelding. The connected parts are then simultaneously formed and quenched. The patch is used in areas, where a reinforcement is needed for higher stiffness. The same principal follows the use of tailor-rolled blanks. These blanks have a variable sheet thickness, which is applied in the rolling process. A different strategy for creating tailored material properties is the use tailor-welded blanks, where different materials are connected before forming via welding. Due to the different chemical composition of the connected materials the microstructural development during the hot forming process is also different [2].

In general, shape distortion is more pronounced with variations of the press hardening process, due to the different volume of the hard phase martensite and the soft phases ferrite, pearlite and bainite. The need for predicting the component geometry after the forming and cooling process as accurate as possible becomes reasonable to avoid extensive use of tool rework and process adaptations. In LS-Dyna the material models **\*MAT\_244** [6] and **\*MAT\_248** [3] are able for predicting the microstructure for hot stamping processes. The material models are calculating the continuous-cooling-transformation (CCT) diagram based on a given chemical composition, while the more advanced **\*MAT\_248** allows a more flexible choice of phase dependent evolution parameters.

## 2 Tailored property process simulation

For the simulation of a tailored property process a hot forming process for an automotive b-pillar is considered. The blanks are fully austenitized at over 900° C and are then transferred to the forming tool. In the lower part of the b-pillar, a heated tool region is used to avoid the martensitic transformation. The temperature of the heated tool is about 550° C, while the upper part is water-cooled. In the upper water-cooled area, the austenite transforms into martensite, while at the heated tool area, a soft ferrite-pearlite microstructure develops through the slower cooling rates. Characteristic for tailored property processes is the evolution of transition zones, where the material shows a gradient from the soft to the hard phases. Especially bainite is existent in the transition zone. Nevertheless, the width and final microstructure of the transition zone is dependent of the heated tool temperature. The causal relationships were investigated e.g., by Feuser [7]. Figure 1 shows the b-pillar with the upper hard area and the soft bottom area. Yield curves show the characteristic material behavior of the different zones of the b-pillar.

For a holistic process simulation, a multistage approach was chosen with the single stages forming (OP 10), quenching (OP 20), springback (OP 30) and cooling (OP 40). After each simulation the stress-strain state and the temperatures of the shell elements of the blank were written to dynain files. For an accurate representation of the temperature state, thermal shell elements were applied. For the forming and quenching simulation, the LS-Dyna explicit solver was chosen, while for the springback and cooling simulation the implicit solver was used. For all simulation stages, the thermo-mechanical solver of LS-Dyna was used. An element length of around 1.5 mm was chosen to account for the accurate representation of the tool radii. For the simulation the material models **\*MAT\_106** and **\*MAT\_248** were considered. The material model **\*MAT\_106** can predict the temperature dependent viscoplastic behavior but lacks to model the occurring phase transformations existent in the forming process. This phase transformation kinetics can be modelled with the material model **\*MAT\_248**, which is suited to model the hot forming of steel.

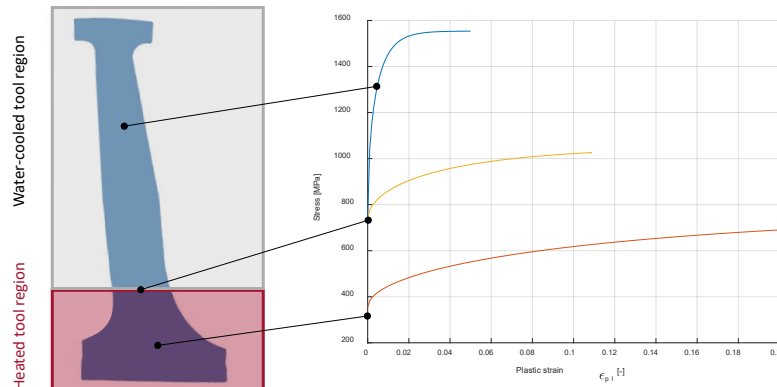


Fig.1: Characteristic mechanical behavior in different zones of a b-pillar, which is produced by a tailored property process.

The main material input parameters for the material model **\*MAT\_248** are:

- The chemical composition of the underlying steel alloy (cards 3 and 4). Based on the heuristic formulas by Watt et al. [10] the starting temperatures for the different phase transformations are calculated.
- The latent heat for the decomposition of austenite into ferrite, pearlite, bainite (LAT1) and martensite (LAT5).
- The activation energies for the diffusive transformation of austenite into ferrite (QR2), pearlite (QR3) and bainite (QR4).
- The ASTM grain size parameter (GRAIN) for the initial austenite grain size.
- The yield curves for the microstructures austenite (LCY1), ferrite (LCY2), pearlite (LCY3), bainite (LCY4) and martensite (LCY5). Strain rate and temperature dependence can be considered with a tabulated input.
- Phase and temperature dependent input of the Young's modulus (E), the thermal expansion coefficient (TABTH) and densities (TABRHO).
- Additionally, the evolution parameters at cards 10 and 11 allow a fine tuning of the different phase evolution for the fit to the CCT diagram. A cooling rate dependence can be considered here.

For the modelling of a tailored property process the material parameters for the critical cooling rate (DTCRIT) and sampling interval (TSAMP) detect a holding phase at the heated tool region. For conventional press hardening process the hardness is calculated by empirical equations after the transformation of austenite [6]. When a holding phase is detected by DTCRIT and TSAMP this hardness calculations is switched to an incremental formulation. The hardness is then calculated by the load curves for bainite (LCH4) and martensite (LCH5), which relate the resulting Vickers hardness to the current temperature.

### 3 Parameter identification

Table 1 shows the main alloying elements of the 22MnB5 steel material with aluminum silicon coating. The b-pillar has a thickness of around 1.60 mm. Figure 2 illustrates the CCT diagram of a 22MnB5 alloy [8,9]. The red cooling curve of 25 K/s is the critical cooling rate for the full martensitic transformation of the austenitized material.

C	Mn	Si	Cr	Al	B
0.221	1.263	0.285	0.146	0.05	0.0037

Table 1: Chemical composition of the blank material

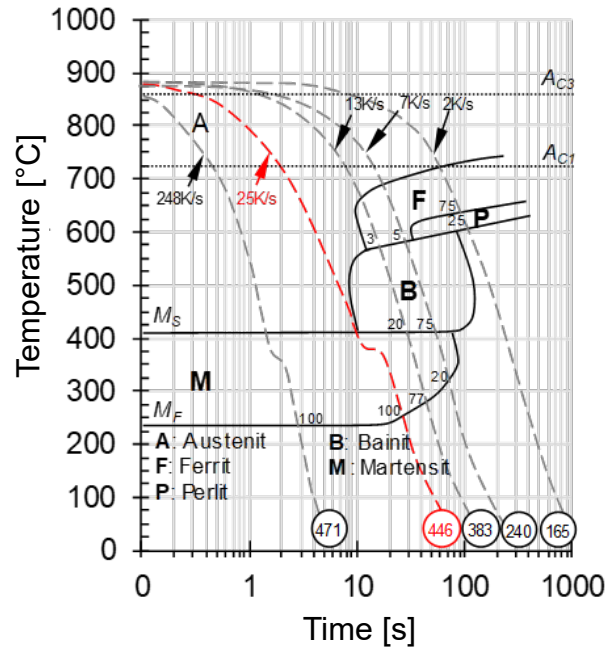


Fig.2: CCT diagram for 22MnB5 [8,9].

The chemical composition was directly inserted in the material cards for **\*MAT\_248**. A set of five 1-element simulations was used to determine the phase transformation behavior of the material model. The five different cooling rates from the CCT diagram in figure 2 were implemented. The cooling rates of 248 K/s and 25 K/s show a full martensitic transformation (100 %). The cooling rates of 13 K/s and 7 K/s have a mixed microstructure with different amounts of ferrite (3/5 %), bainite (20/75%) and martensite (77/20 %). The slowest cooling rate of 2 K/s led to a soft microstructure consisting of ferrite (75 %) and pearlite (25 %) after cooling to room temperature.

To evaluate the influence of the different material parameters on the transformation behavior, a sensitivity analysis was performed with LS-Opt. The objective function  $F(\boldsymbol{\kappa})$  for the optimization problem is the minimization between the phase fractions in the CCT diagram  $u_i^{cct}$  and the predicted phase fractions  $u_i(\boldsymbol{\kappa})$  for the 1-element simulations by the material model **\*MAT\_248**:

$$F(\boldsymbol{\kappa}) = \frac{1}{n} \sum_{i=1}^n (u_i(\boldsymbol{\kappa}) - u_i^{cct})^2 \rightarrow \min. \quad (1)$$

Where  $\boldsymbol{\kappa}$  is the vector of the design variables consisting of the activation energies (QR2, QR3, QR4), the grain size parameter (GRAIN) and the latent heats (LAT1 and LAT5). The parameters were varied in a range of  $\pm 20$  % to their baseline value from the LS-Dyna Manual Volume II [11]. The biggest influence on the resulting phase fractions  $u_i(\boldsymbol{\kappa})$  have the activation energies QR2, QR4 and QR3. The ASTM grain size number is dependent on the austenitization time and especially the holding time over the austenite end temperature  $A_{c3}$  [7]. An increased ASTM grain size number is equivalent to shorter holding times and a reduced average grain size in  $\mu\text{m}$ . Moreover, an increased ASTM grain size number influences the simulated microstructure, respectively leads to a different influence of the activation energies for the material model **\*MAT\_248**. The results of the sensitivity analysis are summarized in figure 3, where you can see the difference of the sensitivity results by varying the range for the considered ASTM grain size number.

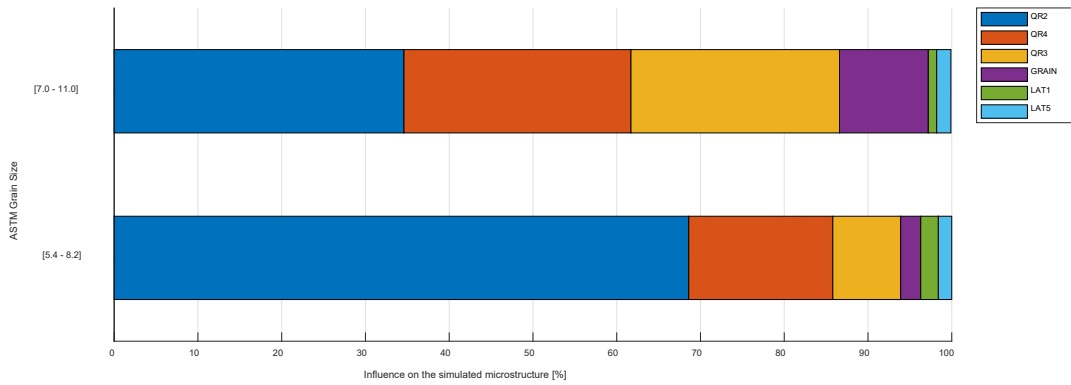


Fig.3: Sensitivity analysis for the 1-element simulations. Bottom: Influence on the simulated microstructure for variation of the baseline values from the LS-Dyna Manual. Top: Change of the sensitivity results, due to an increased ASTM grain size parameter.

The grain size influence is especially pronounced for moderate cooling rates around 10 K/s, where the respective phase vol % is controlled by the initial austenite grain size. The effect of the grain size for the phase transformation can be seen in figure 4, which was determined for the chemical composition of table 1 with the thermodynamic calculation program JMatPro. For the ASTM grain size of 8.0 a cooling rate of 10 K/s leads to an amount of more than 80 % of martensite. While for the ASTM grain size of 11.0 the same cooling rate leads to an amount of almost 70 % of bainite. An ASTM grain size of 8.0 is equivalent to an average grain size of 22.1  $\mu\text{m}$ , while an ATSM grain size of 11.0 is an average grain size of 7.8  $\mu\text{m}$ . An increased former austenite grain size leads to a delayed transformation of ferrite, pearlite and bainite and in this way results in an increased amount of martensite. This is due to the reduced number of nucleation sites during the phase transformation. This emphasizes the accurate chose of the initial austenite grain size, which was therefore determined experimentally.

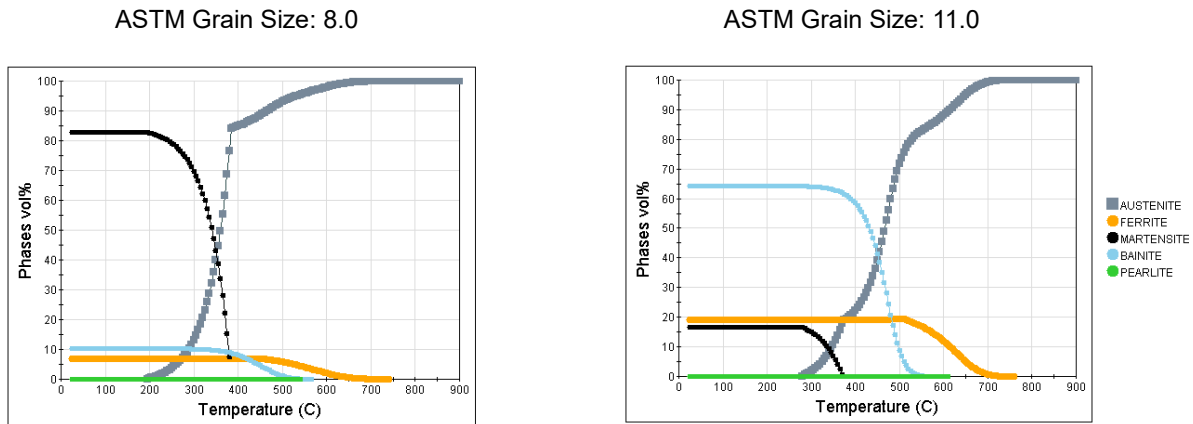


Fig.4: Influence of the initial austenite grain size on the phase transformation for a cooling rate of 10 K/s calculated with JMatPro.

The initial austenite grain size is a process dependent variable, which was determined by EBSD measurement of the martensitic structure of the final part. According to the literature, the former austenitic grains show certain misorientation angles (20° to 49°) [9,12]. With the inverse pol figure coloring the grain structure and crystal orientation was determined. From these images the grain boundaries with the misorientation between 20° and 49° degree were filtered. Afterwards, horizontal, vertical, and diagonal cuts were placed at the filtered image and at the intersection between the cutting lines and grain boundaries the grain sizes were determined. Then a mean value for the grain size was calculated for every cutting line. Subsequently the former austenite grain size was the mean value of all cutting lines for the investigated sample. Figure 5 shows the workflow for the grain size determination, which was proposed by Andreiev [9].

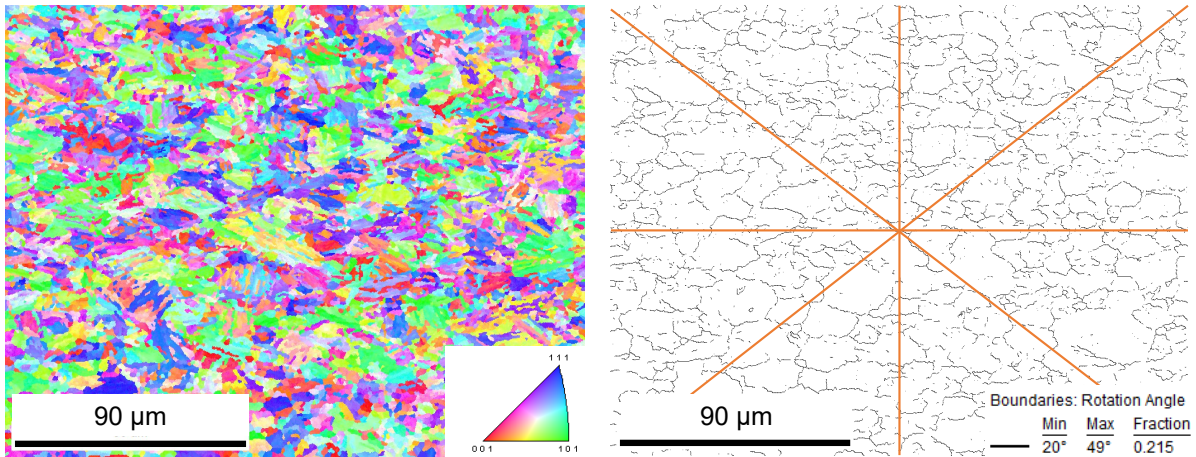


Fig.5: Determination of the former austenite grain size for the considered tailored property process. Left: Inverse pole figure coloring for the grains. Right: Cutting lines to determine the former austenite grain size.

After the experimental determination of the austenite grain size, the optimization problem defined in equation (1) was reduced to the optimization of the values for the design variables QR2, QR3 and QR4. A metamodel based optimization strategy with a sequential domain reduction was chosen. The considered range of the activation energies was increased to  $\pm 50\%$  of their baseline value. In this way, the parameters for the activation energies were identified.

In figure 6 you can see the development of the Vickers hardness over time for the five 1-element simulations. Compared to the experimental CCT diagram in figure 2 they show a good agreement for the prediction of the resulting Vickers hardness. Moreover, a good fit between the microstructural composition was established with the 1-element simulations.

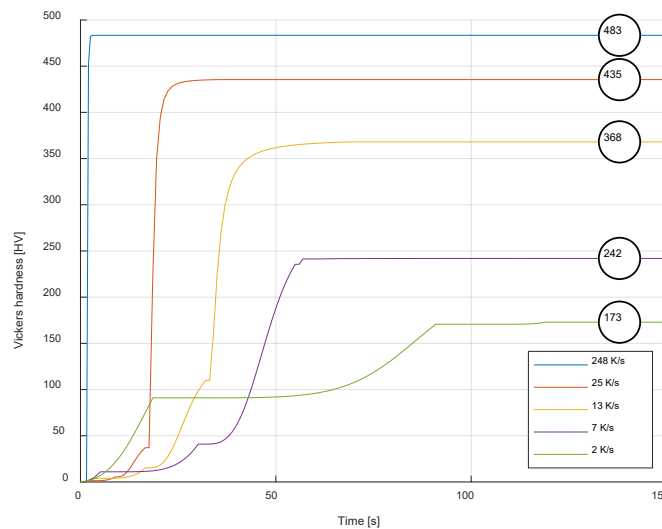


Fig.6: Vickers hardness over time for the different cooling rates with 1-element simulations for the optimized parameter set of the activation energies.

As mentioned in chapter 2, the hardness of the heated b-pillar area is dependent on the quenching time and the temperature of the heated tool region. Higher temperatures lead to the formation of upper bainite and/or ferrite-pearlite, while lower tool temperatures favor the formation of lower bainite. At the upper bainite formation, the diffusion of the carbon atoms at the grain boundary is still possible, which leads to pearlite like microstructure. For lower bainite the diffusion of the carbon atoms is reduced, which enforces a more martensitic like microstructure. Lower bainite has a higher hardness than upper bainite, although the boundary between the two microstructures is blurred [7]. The material model **\*MAT\_248** is not able to differ between the formation of upper or lower bainite. Nevertheless, as described in chapter 2 the parameters DTCRIT and TSAMP allow the detection of a holding phase for the tailored property

process. The load curve LCH4 for the calculation of bainite Vickers hardness over tool temperature needs to be defined for an accurate prediction of the resulting hardness. Moreover, the transformation kinetics of the austenite during hot forming processes is influenced by an existing plastic deformation. For a plastic deformation of 0.2 the start of the bainitic transformation is delayed compared to an elastic deformation state [14]. This effect can be considered in the material model **\*MAT\_248**. With the load curve LCEPS4 the bainitic activation energy QR4 can be scaled dependent on the present plastic strain. To summarize, the tailored property process relevant parameters respectively load curves DTCRIT, TSAMP, LCH4 and LCEPS4 need to be determined.

Based on the temperature evolution during the four different simulation stages described in chapter 2, three simplified time-temperature process routes were defined to characterize the relevant material parameters especially in the heated tool area, see figure 7. The route 1 was defined by the temperature distribution for the soft zone of the b-pillar. While the route 2 was represented by the transition zone of the of the b-pillar. Furthermore, a temperature route with added plastic strain of 0.0, 0.1 and 0.2 was considered. With a developed digital image correlation (DIC) setup the strain and temperature fields were coupled in conventional tensile testing machine. Tensile testing samples were fully austenitized by inductive heating. After a certain holding time, the controlled cooling shown in figure 7 was done. The different cooling rates were established via regulated air cooling [13]. Afterwards, the resulting microstructure was determined by microscopic measurements.

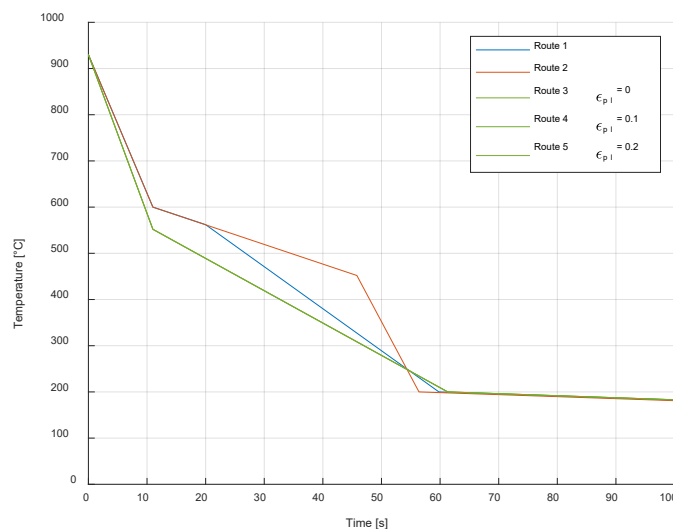


Fig.7: Time-temperature diagram for five characteristic process routes of the tailored property process.

Again 1-element simulations with the time-temperature profile of figure 7 were used to investigate the predicted microstructure by the material model **\*MAT\_248**. The parameter identification approach was similar as described in equation (1). Figure 8 shows the comparison between the experimental and virtual results for the microstructure for the time-temperature curves shown in figure 7. The material model was able to predict the resulting hardness accurately. Process route 3 showed an amount of 79 % bainite for the experimental investigation of the microstructure. The material model was predicting an increased amount of martensite (33 %) and therefore a reduction of the bainite phase vol % (67 %). For the process routes 4 and 5 the added plastic strain led to an increased amount of bainite and therefore to a softer microstructure, which was also correctly calculated by the optimized material model **\*MAT\_248**. For the process route 1 the material model predicted an amount of 54 % martensite and 46 % of bainite, whereas the experimental investigations showed an increased amount of bainite (73 %). For the process routes 2, 4 and 5 the material model showed a full bainitic transformation as seen by the experiments. The deviations are probably related to the CCT diagram taken from literature in figure 2, which was used to optimize the activation energies, but is not determined for the unique chemical composition in table 1 and the investigated ASTM grain size number.

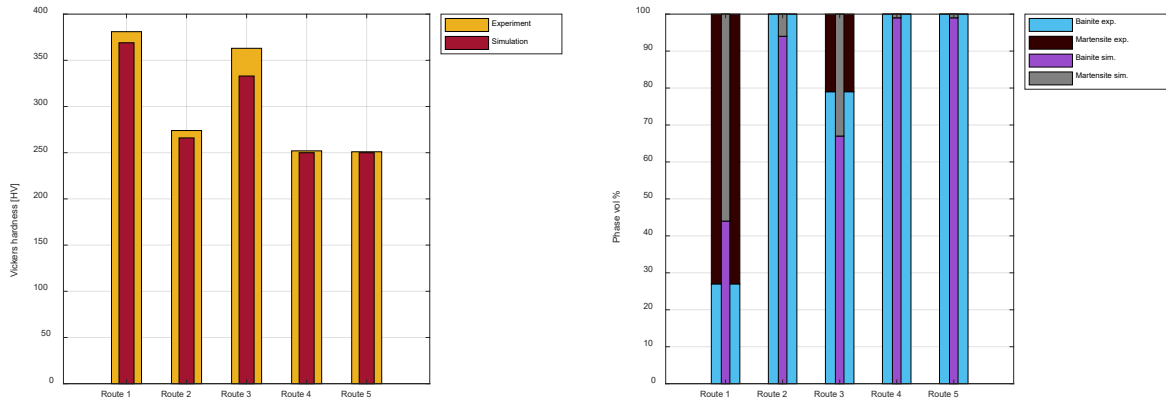


Fig.8: Left: Comparison of the experimental and virtual hardness for the time-temperature process routes from figure 7. Right: Experimental results for the phase fractions of bainite and martensite.

#### 4 Process simulation

After the parameter identification based on 1-element simulations and experimental investigations, the optimized material model was considered for the multi-stage forming simulation of the b-pillar described in chapter 2. As shown for the simulations and experiments in chapter 3, the same microstructural investigations were done for the b-pillar. Therefore, samples were cut out from the final part geometry and the phase fractions and hardness was measured. Close attention was focused on the transition area from the soft heated region to the upper martensitic part of the b-pillar. Moreover, samples were cut at designated soft and press hardened areas. Figure 9 shows the hardness of the transition area for the experimental data and the predicted hardness by the material model **\*MAT\_248** after the cooling simulation (OP 40). Due to the length of the transition area of about 50 mm, the results are sensitive to the chosen element length for the initial simulation. The trend of the microstructure development in the transition area was well predicted by the material model **\*MAT\_248**.

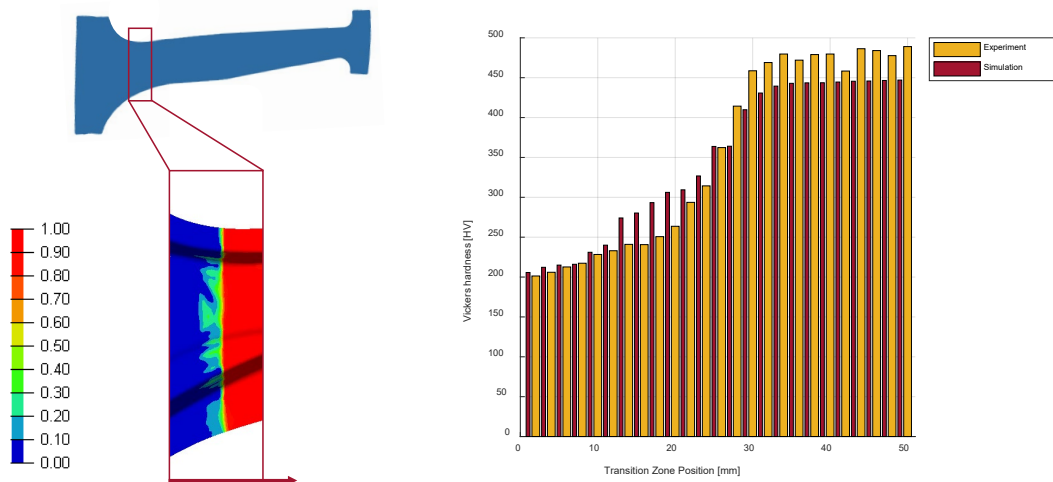


Fig.9: Comparison of the microstructure in the transition zone of the b-pillar for the experimental and simulated data.

The final parts of the b-pillar were optical scanned and compared to the simulated results. To account for the sheet thickness, the shell elements were transformed to solid elements beforehand. The experimental results were compared to the simulated results for the b-pillar with the material models **\*MAT\_106** and **\*MAT\_248**. Figure 10 shows the results for the optical scanned and simulated b-pillars. The reference part is the simulated part, and the mm scale shows the difference to the optical scanned results. It was shown that with the material model **\*MAT\_248** a better prediction of the final geometry can be established. For now, post forming operations are not considered yet e.g., laser cutting.

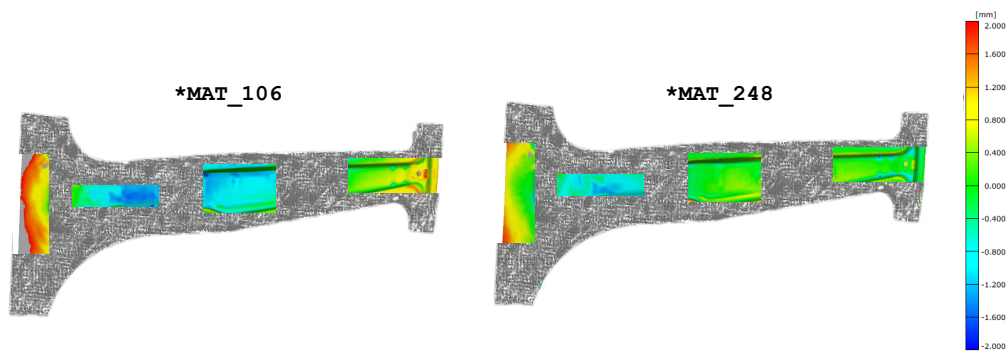


Fig.10: Comparison of the optical scanned b-pillar compared to simulated results for the material model \*MAT\_106 and \*MAT\_248.

## 5 Summary and Outlook

The presented study showed an approach for the modelling of tailored tempering parts. The focus was the prediction of the final microstructure and geometry of the formed components. Due to the coexistence of different steel phases for the tailored property process, the final parts are more prone to distortion. Therefore, an accurate prediction of the geometry by FEM simulations can reduce rework cycles for the involved forming tools.

A strategy was shown how the parameter identification for the material \*MAT\_248 can be done. With simple 1-element simulations and a performed sensitivity analysis the influence of different material parameters was investigated. Based on the simulative results the parameter for the former austenite grain size was determined experimentally. The activation energies for the microstructures ferrite (QR2), pearlite (QR3) and bainite (QR4) were optimized to predict the CCT diagram shown in figure 2 accurately. Moreover, the relevant parameters for the modelling of tailored tempering processes were identified by the consideration of different time-temperature process routes, see figure 7. Moreover, the influence of plastic deformation on the bainitic activation energy (QR4) was examined in this way.

Afterwards, the optimized material model \*MAT\_248 was implemented in the multistage forming simulation of the tailored property process. The simulation with the single stages forming (OP 10), quenching (OP 20), springback (OP 30) and cooling (OP 40) allows the modelling from a fully austenitized state to a cooling down to room temperature. For the final b-pillar the resulting microstructure was compared to the predicted microstructure by the material model \*MAT\_248. Moreover, the simulated geometry was compared to the part geometry after the forming operation. It was shown, that with the material model \*MAT\_248 a better prediction of the final part geometry can be established, compared to the material model \*MAT\_106.

Nevertheless, the results can still be improved. Further suitable research activities are:

- Consideration of additional process operations e.g., laser cutting.
- The optimization of the activation energies was done for a CCT diagram from literature. An improved prediction can be reached by considering the CCT diagram for the exact chemical composition, ASTM grain size number and austenitization temperature. This diagram can be determined experimentally or calculated e.g., by JMatPro.
- The evolution parameters of the material model \*MAT\_248 for the different phases were kept to their baseline value. In general, the phase transformation evolution parameters show a cooling rate dependence, which can be considered.
- The tool temperatures of the heated and cooled region are currently considered only by two different temperatures, which of course is a simplification of the real process temperatures. Since, the temperatures of the water and the heating cartridges are tracked, a solid element simulation of the involved tools can lead to more accurate prediction of the surface temperatures.

## 6 Literature

- [1] Neugebauer R, Altan T, Geiger M, Kleiner M and Sterzing A: "Sheet metal forming at elevated temperatures" CIRP Annals 55, 2006, 793–816
- [2] Mori K, Bariani P F, Behrens B-A, Brosius A, Bruschi S, Maeno T, Merklein M and Yanagimoto J: "Hot stamping of ultra-high strength steel parts", CIRP Annals 66, 2017, 755–77
- [3] Hippchen P: "Simulative Prognose der Geometrie indirekt pressgehärteter Karosseriebauteile für die industrielle Anwendung", Erlangen-Nürnberg, Univ., Diss., (Bamberg: Meisenbach), 2014
- [4] Audi Media Center. [www.audi-mediacycenter.com/de/elektro-suvs-im-premium-kompaktsegment-der-audi-q4-e-tron-und-der-q4-sportback-e-tron-13887/karosserie-und-aerodynamik-13899](http://www.audi-mediacycenter.com/de/elektro-suvs-im-premium-kompaktsegment-der-audi-q4-e-tron-und-der-q4-sportback-e-tron-13887/karosserie-und-aerodynamik-13899) (accessed August 25, 2021)
- [5] Marten T: "Erweiterung des Portfolios presshärterbarer Stähle durch gezielte Werkstoff- und Prozessmodifikationen" Schriftenreihe / Institut für Leichtbau mit Hybridsystemen, Band 27/2017, Aachen: Shaker Verlag 2017
- [6] Åkerström P, Bergman G and Oldenburg M: "Numerical implementation of a constitutive model for simulation of hot stamping" Modelling and Simulation in Materials Science and Engineering 15, 2007, 105–119
- [7] Feuser P S: „Ein Ansatz zur Herstellung von pressgehärteten Karosseriekomponenten mit maßgeschneiderten mechanischen Eigenschaften: Temperierte Umformwerkzeuge, Prozessfenster, Prozesssimulation und funktionale Untersuchung“ Bericht aus dem Lehrstuhl für Fertigungstechnologie / Univ. Erlangen-Nürnberg, Bd. 226. Bamberg: Meisenbach 2012
- [8] Naderi M: "Hot stamping of ultra high strength steels" Aachen, Techn. Hochsch., Diss., 2007
- [9] Andreiev A: „Kurzzeitaustenitisierung höchstfester Stähle - eine zeiteffiziente Methode zur Fertigung sicherheitsrelevanter Bauteile mit verbesserten Eigenschaften“ Universität Paderborn, Diss., 2020
- [10] Watt D F, Coon L, Bibby M, Goldak J and Henwood C: "An algorithm for modelling microstructural development in weld heat-affected zones (part a) reaction kinetics" Acta Metallurgica 36, 1988, 11, 3029–3035
- [11] LTSC: "LS-DYNA Keyword User's Manual – Volume II: Material Models", Livermore, 2021
- [12] Suikkanen P P, Cayron C, DeArdo A J and Karjalainen L P: "Crystallographic Analysis of Martensite in 0.2C-2.0Mn-1.5Si-0.6Cr Steel using EBSD" Journal of Materials Science & Technology 27, 2011, 920–930
- [13] Reitz A, Grydin O and Schaper M: "Phase Transformation Characterization by Means of High Temperature Digital Image Correlation for Graded Thermo-Mechanical Processing of Sheet Parts" Characterization of Minerals, Metals, and Materials 2020, 69–79
- [14] Schaper M, Gershteyn G, Grydin O, Fassmann D, Yu Z, Nürnberger F: "Modellierung des Werkstoffverhaltens beim Warmumformen höchstfester Stähle auf der Basis mikrostruktureller Vorgänge" Tagungsband zum 5. Erlanger Workshop Warmblechumformung, 2010, 141–162